Electronic Supplementary Material

Substrate mediated dissolution of redox active nanoparticles; electron transfer over long distances

Ruo-Chen Xie, Christopher Batchelor-McAuley, Minjun Yang, and Richard G. Compton (✉)

[1] *Department of Chemistry, Physical and Theoretical Chemistry Laboratory, University of Oxford, South Parks Road, Oxford OX1 3QZ, UK*

Supporting information to https://doi.org/10.1007/s12274-021-3497-6

1. TEM images and sizing of the silver nanoparticles

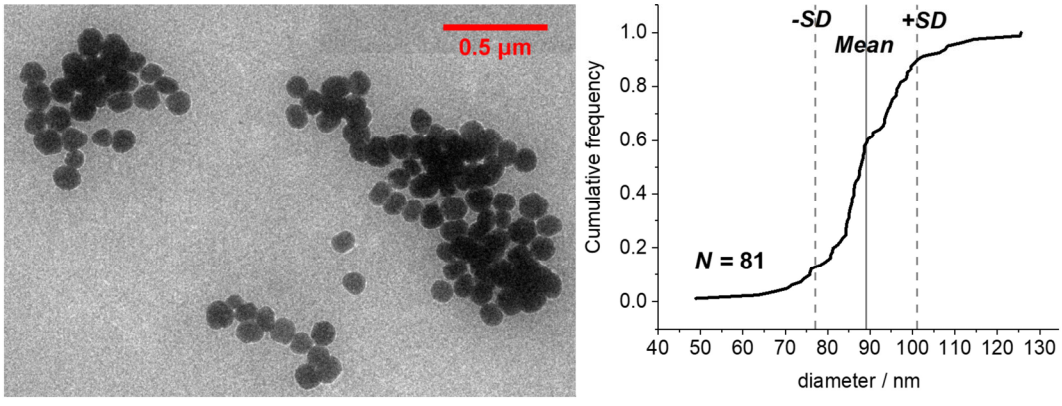

Figure S1 TEM image of the nominally 100 nm Ag NPs and their size distribution. Mean diameter with standard deviations is marked by the vertical lines.

2. Microscopy set-up for reflective dark field illumination and optical intensity measurements

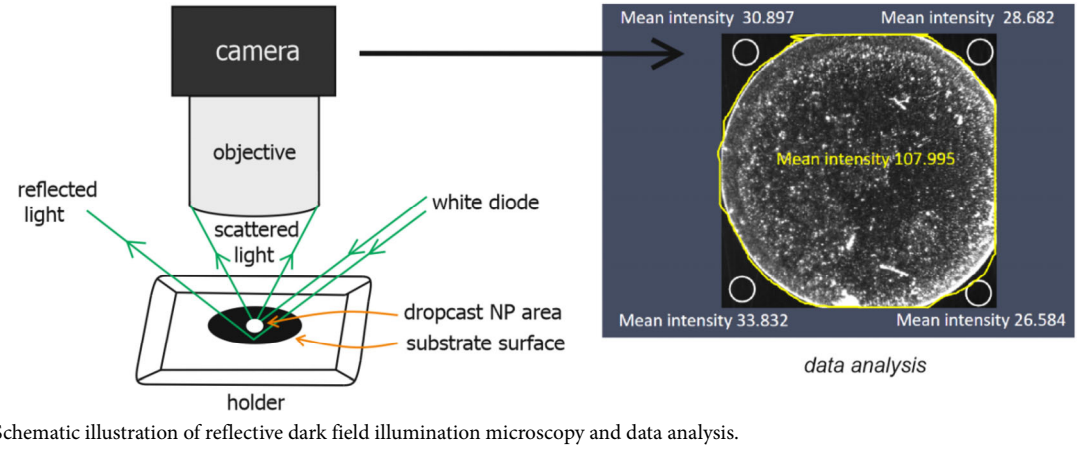

Figure S2 Schematic illustration of reflective dark field illumination microscopy and data analysis.

Figure S2 in the ESM shows the microscopy set-up for the optical measurements under reflective dark field illumination. The position of the substrate is held fixed by a holder and exposed to the objective above. A white diode light source is maintained in a fixed position from which the incident light is directed to the substrate surface at an angle from the above. Consequently, in contrast to the light reflected away by the flat and smooth substrate surface which therefore appears minimal light intensity at the corners of the produced image, the silver nanoparticles located in the in-focus dropcast area scatters light which partly enters the objective and so this central area appears very bright.

Using the camera, the image described above is obtained and the optical intensity is analysed. Specifically, the mean light intensities over the whole central dropcast area (I_{tot}) highlighted by the yellow outline and the bare substrate at the corners (I_s)

Address correspondence to richard.compton@chem.ox.ac.uk

were measured respectively. Assuming the substrate scatters homogeneously across the whole imaged area, the scattered light intensity from the Ag nanoparticles was thus measured by subtracting the average I_s over the four corners from the I_{tot}.

3. Optical analysis of the scattering features from a glassy carbon surface

In this section we report the individual scattering features observed on the electrode surface.

First, a total number of 23 separate bright scatters were selected as the representative features on the basis that their half maximum intensity (29 ± 6 a.u.) is approximately the mean intensity (31 a.u.) of all the particles across the drop-cast area. Five of them in a local region of Figure 3a are presented in Figure S3 a and clear images of their individual spreading scattering are shown in Figure S3 b-f. The scattering appears quasi-spherical with a central maximum intensity. Note that here we only focus on the Airy-type diffraction pattern resulting from the circular aperture of the objective; therefore the four-spike diffraction patterns forming upon the additional light diffraction by the square-shaped aperture of the camera sensor is avoided in the following measurement of the line-profile intensity for accuracy. The line profiles of intensity distribution across the selected optical features, e.g. that of Feature 1, were plotted (Figure S3 g), from which the full widths at half maximum (FWHM) were measured, giving an average value of 2.0 ± 0.2 μm (Figure S3 h). This value is used as the approximate mean size of all the observed scattering features.

Due to the Abbe diffraction limit of an optical system using a visible light source, the size of the scattering spots of a single 100 nm-diameter spherical NPs is expected to be significantly larger than their own geometry size. Previous work [S1] has simulated the point spread function of the optical microscopy. According to the equations given in that work

$$l_0 = \alpha\sqrt{|\log(\frac{1}{4})|} \tag{1}$$

where l_0 is the radius at half maximum of the point spread function of the particles, and $\alpha \sim 0.435\frac{n\lambda}{2NA}$ [S1] (λ is the wavelength of incident light, here we take 550 nm as the average wavelength for the white light source, n is the refractive index of the medium (~1.33) and NA is the numerical aperture of the microscope objective). Accordingly the expected FWHM of the diffraction limited pattern for a single nanoparticle is calculated to be 0.7 μm. This is significantly smaller than the measured mean size of 2.0 ± 0.2 μm. It follows that the drop-cast nanoparticles in fact form large surface clusters due to the particle agglomeration during the electrode drying process.

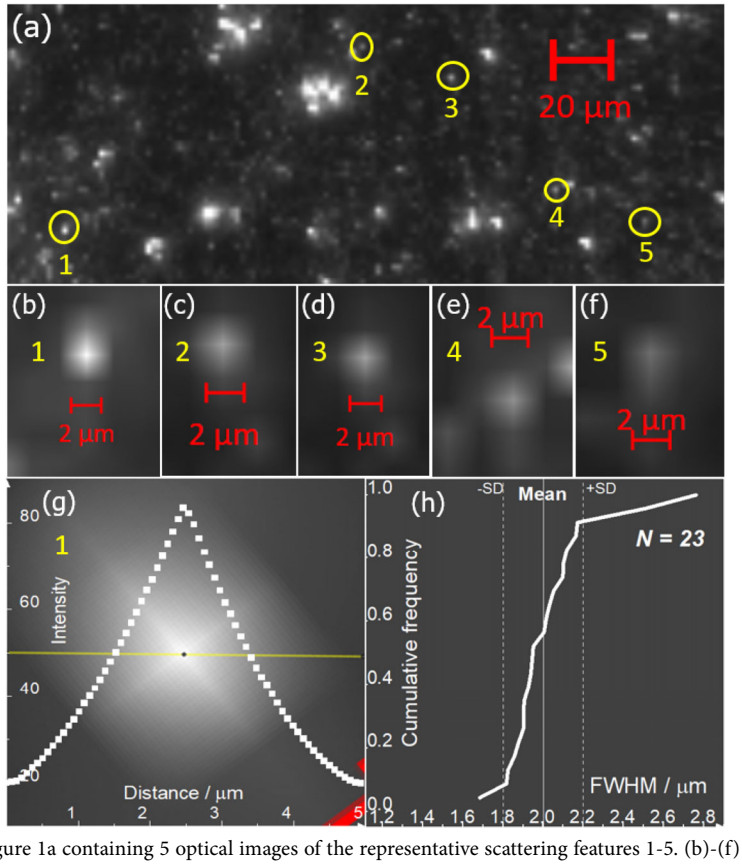

Figure S3 (a) Local region of Figure 1a containing 5 optical images of the representative scattering features 1-5. (b)-(f) Scattering patterns of individual optical features. (g) Line profile of the scattering intensity across Feature 1. (h) Size distribution of the 23 optical features. The mean FWHM with standard deviations is marked by the vertical lines.

4. Reproducibility of the measured mean scattered light intensity of dropcast Ag NPs

To evaluate the reproducibility of the mean intensity of the scattered light from the dropcast silver particles, the measurements were repeated for five times. On glassy carbon surfaces, as the light intensity of the substrate corners was kept at around 31 a.u.,

the total scattering intensity of the five drop-cast areas with different surface morphology (see Figure S4 in the ESM) was measured to range from 107 to 138 a.u. Consequently, the mean scattered light from Ag NPs averaged over these five repeats are calculated to be 85 ± 15 a.u., indicating an 18% reproducibility. Similarly, on all the other substrates used in this work, the reproducibility is found to be around 20% as shown in Table S1.

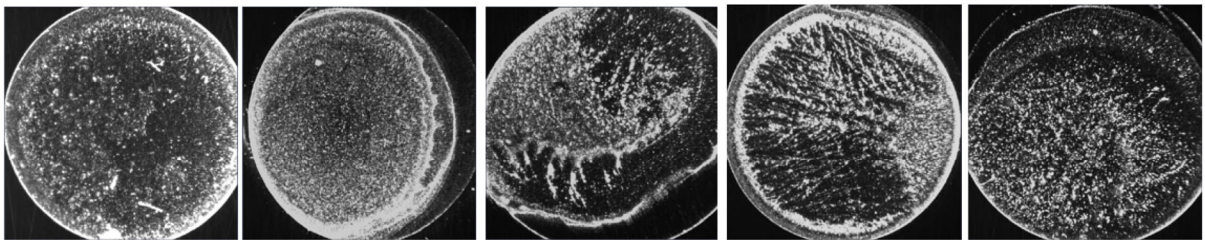

Figure S4 Images of the drop-cast areas in 5 repeat experiments on a glassy carbon surface.

Table S1 Particle scattering light intensity in 5 repeat experiments on the different substrates.

Sample code	Total intensity	Substrate intensity	NP intensity	Mean±SD and SD/mean ratio
GC1	108	30	78	
GC2	126	33	93	
GC3	104	33	71	85 ± 15 (18%)
GC4	138	31	107	
GC5	107	31	76	
Glass1	114	39	75	
Glass2	119	42	77	
Glass3	99	43	56	73 ± 15 (21%)
Glass4	135	40	95	
Glass5	102	40	62	
ITO1	67	26	41	
ITO2	72	25	46	
ITO3	60	28	32	37 ± 7.1 (19%)
ITO4	57	29	28	
ITO5	64	26	38	
Pt1	66	29	37	
Pt2	63	27	36	
Pt3	55	30	25	35 ± 6.0 (17%)
Pt4	65	26	39	
Pt5	67	27	40	

5. Effects of electrode washing by deionised water on the scattering pattern and intensity

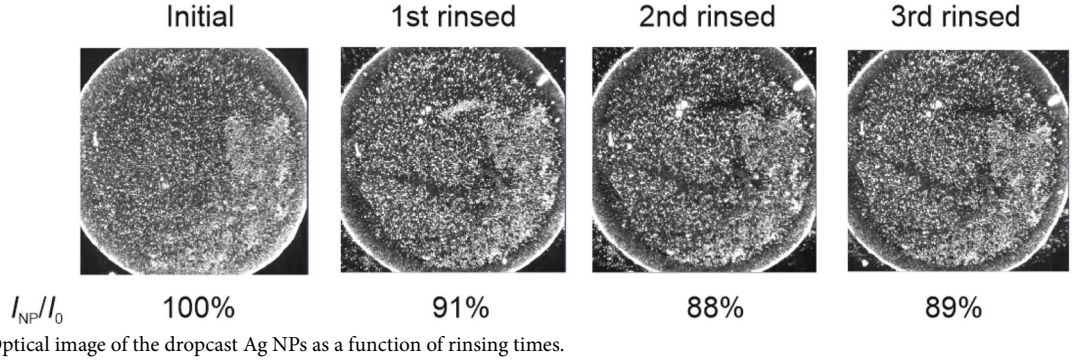

Figure S5 Optical image of the dropcast Ag NPs as a function of rinsing times.

6. SEM imaging of the dropcast silver nanoparticles after immersion in water and in iodide solutions

To examine the fate of the dropcast silver nanoparticles, mainly the presence or absence of solid particles on the NP-modified substrate surfaces, after immersion in iodide solutions, SEM imaging of the silver nanoparticles supported on GC and glass

substrates after immersion in water or in the iodide solution was conducted. Specifically, GC and glass substrates were first thoroughly cleaned by immersing in Aqua Regia for 1 hour, and the silver nanoparticles were dropcast onto the two substrates, respectively, with a same surface coverage ($2.4\pm0.3 \times 10^8$ nanoparticles cm^{-2}) as that used in this work and dried. Next, the NP-modified substrate surfaces were immersed in deionised water or a 0.2 M KI solution for 6 minutes. For the latter, the substrate surfaces were subsequently rinsed with deionised water. The modified substrate surfaces were dried under a nitrogen atmosphere overnight. Finally, the particles were located and imaged using SEM (Sigma 300, FEG-SEM, Zeiss) with an accelerating voltage of 2.0 kV at representative sites.

Figure S6 a shows after immersion in water many (herein 86 in total) individual particles with a diameter of mainly 150-200 nm in most imaging regions of the dropcast area. In addition, very close to the edge of the dropcast area (see Figure S6 b) the presence of micron-sized agglomerates was observed and appear to be formed from the 90 nm-diameter nanoparticles. The surface coverage was estimated to be around 2×10^8 nanoparticles cm^{-2}, which is consistent with the dropcast loading of $2.4\pm0.3 \times10^8$ nanoparticles cm^{-2} with a small loss of the particles due to their physical detachment upon immersion. In stark contrast, after immersion in the iodide solution, as shown in Figure S6 c bare surfaces only are observed! On glass substrates, however, despite the difference in the agglomeration states (single nanoparticles in Figure S6 d and diameter ranges of 100-400 nm in Figure S6 e), no significant difference in the nanoparticle surface coverages is observed between the surfaces after immersion in pure water and 0.2 M KI solutions. Consequently, these observations strongly confirm that the substrate-mediated silver dissolution, rather than the formation of solid AgI particles, is the physical origin of the optical disappearance of the dropcast silver nanoparticles.

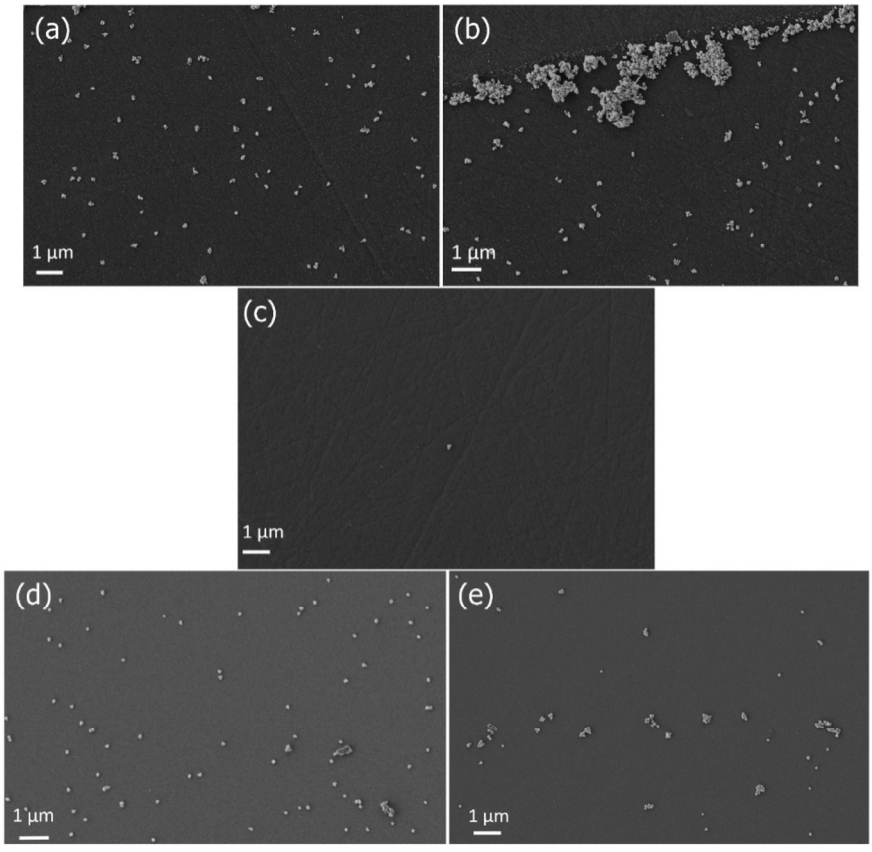

Figure S6 SEM images of silver nanoparticles supported on a glassy carbon surface after immersion in (a) and (b) water or (c) a 0.2 M KI solution for 6 minutes, and those supported on a glass substrate after immersion in (d) water or (e) a 0.2 M KI solution for 6 minutes.

7. Comparison of the substrate potentials for avoiding the nanoparticle dissolution in nitrate solutions with that in iodide solutions

The remaining fraction of scattering as a function of applied substrate potential was also measured in 0.2 M nitrate solutions. It is evident that in this nitrate solution, holding the electrode potential below ca. +0.3 V vs. (Ag/AgCl) can retain over 80% of total scattering whilst the lost 18±4% scattering intensity is very close to that observed when the nanoparticles are exposed to nitrate solutions (i.e. 14±10%, see Figure 5a). In contrast, when the electrode potential is more positive than +0.3 V, more particles are lost from the interface with increasingly positive potentials. Therefore, this clearly shows a substrate potential more negative than +0.3 V is required in the nitrate solutions to avoid nanoparticle dissolution.

For comparison in Figure S7, the overlaid voltammogram of a freshly modified electrode in 0.2 M KNO_3 shows in the forward scan an oxidation peak at +0.31 V, corresponding to silver oxidation to silver ions, whilst in the reverse scan a reduction peak at -0.15 V is seen resulting from the reverse process. The threshold potential above which the oxidation of Ag NPs is observed (+0.25 V) is consistent with that for avoiding the dissolution (<+0.3 V). The latter potential differs significantly from the inhibiting potential in iodide solutions (≤-0.35 marked in the figure below) and the observation of this difference is in excellent agreement with the shift from the threshold potential for the Ag oxidation in 0.2 M KNO_3 (> +0.25 V) to that for the oxidation (>0.33) in 0.2 M KI.

Consequently, the experiments in nitrate solution further shows the sensitivity of the substrate potentials required for avoiding nanoparticle dissolution towards the solution ionic composition.

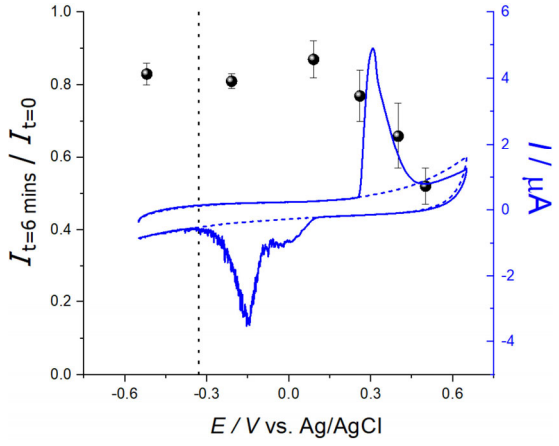

Figure S7 Scatter plots of the average remaining fractions of scattering intensity of the immobilised Ag particles on a GC electrode held at each different fixed potentials after 6 minutes' immersion in an air-saturated 0.2 M KNO_3 solution. The overlaid cyclic voltammograms of (solid) a freshly immersed, modified GC electrode and (dashed) a bare GC electrode in an N_2-saturated 0.2 M KNO_3 solution. Scan rate 0.1 V s^{-1}. Note that in order to facilitate the comparison for different electrolyte conditions, the vertical dashed line labels out the expected electrode potential for Ag/AgI (0.2 M KI), which is consistent with the threshold potential for inhibiting the nanoparticle dissolution under the condition (see main text Section 3.2).

8. Open circuit potential measurements of the silver nanoparticle-modified glassy carbon electrode during the immersion in iodide solutions

We performed the open circuit potential measurements (OCP) of silver nanoparticle modified electrodes in iodide containing solutions over a period of 6 minutes' immersion. Measurements were also made at bare GC electrodes for comparison. Figure S8 a shows that in absence of dropcast nanoparticles, the GC electrode has an almost constant OCP at +0.2 V vs. Ag/AgCl throughout the 6 minutes' immersion in a 0.2 KI solution. However, the silver nanoparticle-modified electrode shows an obvious increase of OCP from -0.15 V to about +0.08 V over the first 60 seconds, and maintains a nearly constant OCP afterwards. The timescale of the change is in good agreement with that of the measured scattering light intensity decrease by optical microscopy where nearly 90% decrease occurred in the first minute, as shown in Figure S8 b. This is not inconsistent with the inferred electrochemical dissolution of silver nanoparticles which is expected to significantly vary the electrode potential.

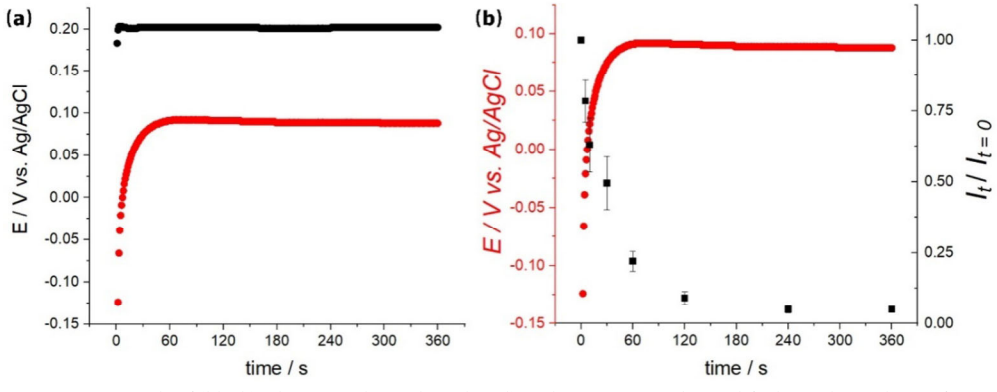

Figure S8 (a) Open circuit potentials of (black) a bare GC electrode and (red) a silver nanoparticle-modified GC electrode as a function of time in 0.2 M KI solutions. (b) Comparison between the changes in the measured OCP and scattering light intensity relative to the initial value over the 6 minutes' immersion in the iodide solution.

9. Calculations of dissolved dioxygen concentration based on the electrochemical sensing

The concentration of dissolved O_2 can be calculated from the voltammetric current of oxygen reduction on a sensing electrode. In O_2 or air saturated solutions, the macroelectrode voltammogram shows irreversible peak currents for oxygen reduction of 30.4±3.4 μA and 8.6±0.7 μA, respectively as described in the main text. The bulk concentrations of dissolved dioxygen in those solutions can therefore be calculated according to Randles-Sevcik equation at 25 °C

$$c^* = \frac{(2.99 \quad 10^5)\sqrt{n' + \beta_{n'+1}} n D^{1/2} A v^{1/2})}{I_p}$$

where c^* is the bulk concentration of O_2, I_p is the peak current, n' is the number of electrons transferred before the rate determining step (n' =0 in this case), $\beta_{n'+1}$ is the transfer coefficient of the rate determining step (discussed below), n is the total number of electrons transferred (n=2), D is the diffusion coefficient (2.69 ×10^{-9} m^2 s^{-1}) [S2] of dissolved O_2, A is the electrode surface area (m^2)

and v is the scan rate (0.05 V s^{-1}). The transfer coefficient $\beta_{n'+1}$ was derived to be 0.31 and 0.27 from the Tafel slope in the region of 20%-30% of the peak current [S3], as shown in Figure S9. Consequently, the O_2 and air saturated solutions are found to contain 1.20±0.10 mM and 0.31±0.02 mM of dissolved dioxygen respectively.

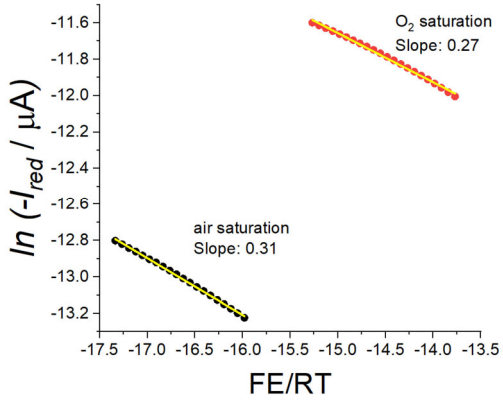

Figure S9 Tafel slopes of oxygen reduction current for air and O_2 saturation conditions.

In the argon-saturated solution, the microelectrode voltammogram shows a quasi-steady-state current of 1.2±0.7 nA. The concentration of oxygen in the bulk solution can therefore be calculated based on the following equation for a cylindrical microwire electrode geometry [S4]

$$c^* = \frac{I_{qss}}{2\pi nFDl(0.446p + 0.335p^{0.15})}, with p = \left(\frac{nFr^2v}{RTD}\right)^{0.5}$$

where I_{qss} is the quasi-steady-state current (A), l and r are the length (m) and the diameter (m) of the microwire electrode, F is the Faraday constant (96485 C mol^{-1}), R is the gas constant (8.314 J K^{-1} mol^{-1}), and T is the measurement temperature (K). Consequently, the bulk concentration of O_2 dissolved in the Ar-saturated solution is calculated to be 1.2±0.7 μM. Similarly, the 2.3±0.4 nA of quasi-steady-state current measured after 6 minutes' aging suggests an oxygen level of 2.3±0.4 μM.

10. Discussions on other possible oxidising agents, protons and triiodide ions

In the main text dissolved oxygen is inferred to be the cause of the particle dissolution. Here we consider other possible oxidising agents notably protons and triiodide ions.

For protons, the possibility of the cell reaction is considered in terms of thermodynamics. The half reaction on the anode is $Ag_{(s)} + I^-_{(aq.)} = AgI_{(s)} + e^-$ (E^o = -0.152 V vs. SHE); therefore, in 0.2 M KI, the anodic potential for the voltaic cell is -0.111 V. For an oxidation involving one I^- ion per Ag atom, the shift in the oxidation potential is +59 mV per unit of $\log_{10}([I^-])$ according to Nernst equation. Therefore, the potential depends on what complexes form upon the oxidation. Nevertheless, it is clear that the anodic potential for the voltaic cell would be more positive than -0.111 V. The half reaction on the cathode is $H^+_{(aq.)} + e^- = ½ H_{2(g)}$ (E^o = 0.00 V vs. SHE). As pH was measured to be around 7 – in between 6.8 (solutions are air-equilibrated after around 30 s) and 7.9 (initially upon gas bubbling), so the concentration of protons is approximately 10^{-7} M. The partial pressure of gas H_2 in the atmosphere is $P_{H2} = 5.55 \times 10^{-7}$ atm [S5]. Using the Nernst equation, the cathodic potential for the voltaic cell is calculated to be -0.229 V vs. SHE. Consequently, due to a negative cell potential the reaction cannot be thermodynamically driven by the H_2/H^+ couple for pH ca. 7.

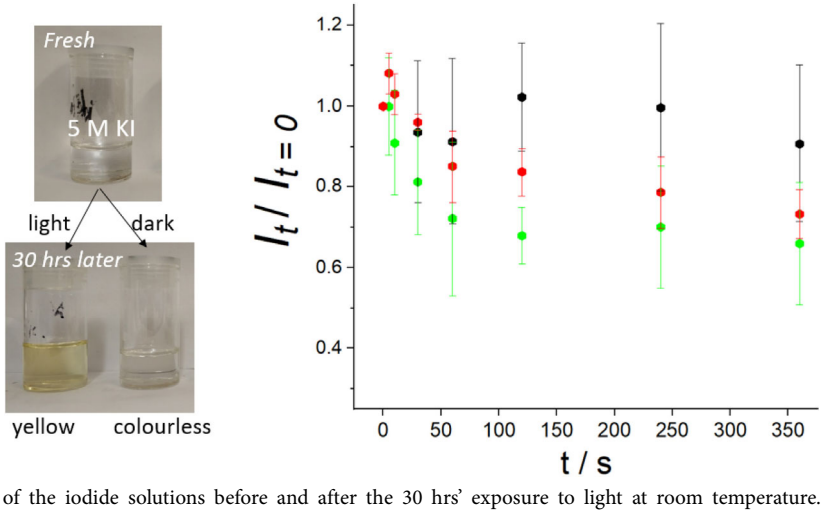

Figure S10 (Left) Colours of the iodide solutions before and after the 30 hrs' exposure to light at room temperature. (Right) Scattering intensity normalised to the initial value of the dropcast Ag NPs on GC substrates as a function of time within the 6 minutes in (black) pure water, (green) a fresh and (red) the aged 0.05 M KI solution, respectively.

I_3^- is not necessarily present in our experiments using iodide solutions fresh (< 3 days) and stored in dark and 4-6 °C, since its presence only becomes visible, by the advent of a yellow colour, after several days at room temperature for 0.2 M KI, following exposure of iodide solutions to light. Nevertheless, we discuss the possibility of it being the oxidising agent for completeness of argument given that thermodynamically the oxidation of silver by tri-iodide is possible ($E^o_{I3-/I-}$ = 0.54 V > $E^o_{Ag/AgI}$ = -0.15 V vs. SHE) [S6].

To clarify the non-involvement of iodine or tri-iodine species present by virtue of the aerial oxidation of the aqueous iodide solutions, we compared fresh and aged solutions. 5 M KI solutions were prepared, which were colourless. The solutions was then exposed to light at room temperature for 30 hrs. As a result, the solution became yellow (see Figure S10 a); in contrast, the solution stored in dark for 30 hrs did not turn yellow. This indicates the presence of triiodide ions in the aged yellow solution. To next compare the dissolution kinetics of interest, the aged solutions were diluted 100 fold to contain 0.05 M iodide but with trace I_3^-. Dissolution experiments were conducted using a fresh and the aged 0.05 M iodide solutions, respectively. Optical intensity of the dropcast Ag NPs was monitored within 6 minutes. As seen from Figure S10 b), no major differences in the dissolution kinetics were observed between the triiodide containing and non-triiodide containing KI solutions. This suggests that in addition to the unlikely presence of I_3^- in our studied solution, the triiodide ions are not considered to be the oxidising agent for our dissolution experiments.

11. Voltammetry of NP-modified electrodes after immersion in the iodide solutions

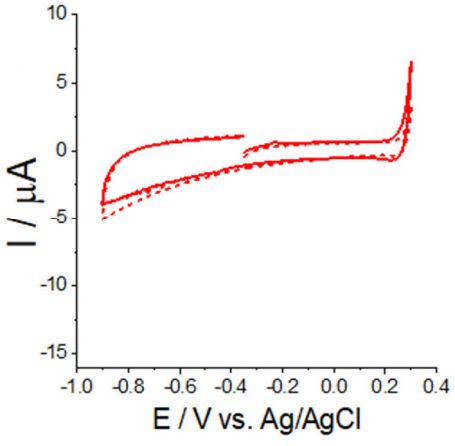

Figure S11 Cyclic voltammograms of (dashed) a bare GC electrode and (solid) an Ag NP-modified GC electrode after the 6 minutes' immersion in a 0.2 M KI solutions. Scan rate 0.1 V s^{-1}.

12. Full-time optical measurements of Ag dissolution kinetics on glass substrates

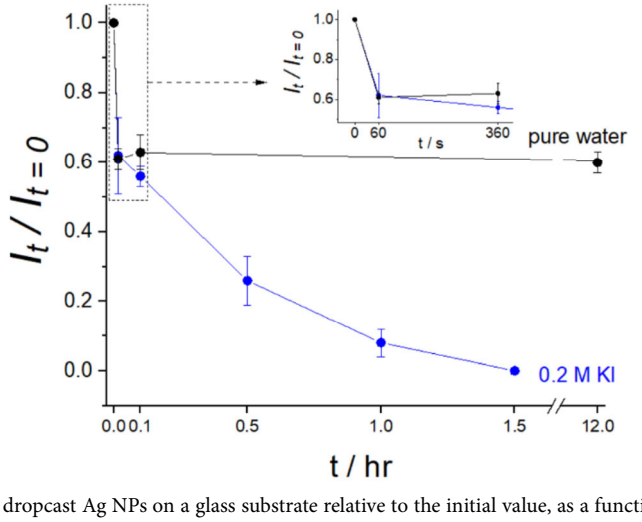

Figure S12 Scattering intensity, of the dropcast Ag NPs on a glass substrate relative to the initial value, as a function of time within the 12 hrs in (black) pure water and (blue) 0.2 M KI solutions, respectively.

13. Calculations for surface area comparison between nanoparticle ensembles and the substrate

The surface areas between the ensembles of the dropcast silver nanoparticles and the substrate are compared based on the following estimation. For a single silver nanoparticle with an average diameter of 90 nm (see SI section 1), the surface area is 2.5×10^{-14} m^2. The amount of dropcast silver nanoparticles is 10 ng, so the number of nanoparticles across the whole dropcast area is calculated to be 2.5×10^6. Therefore, the total surface area of the silver nanoparticle ensemble is 6.4×10^{-8} m^2. For the GC

electrode with a disc diameter of 3.00 mm, the geometric area is 7.1×10^{-6} m^2. The substrate surface used in this work is polished to be very smooth for the reflective dark field illumination, so the roughness factor (ratio of the microscopic area to geometric area) is considered to be below 2 [S7]. Even so, it is evident that despite the large surface-to-volume ratio of nanoparticles, due to the tiny amount of silver to be oxidised, the surface area of GC electrode is substantially larger (2-3 higher orders of magnitude) than the total surface area of all the silver nanoparticles across the dropcast area.

References

[S1] C. Batchelor-McAuley, C. A. Little, S. V. Sokolov, E. Kätelhön, G. Zampardi, R. G. Compton, *Anal. Chem.* **2016**, *88*, 11213-11221.
[S2] Y. Guo, M. Yang, R.-C. Xie, R. G. Compton, *Chem. Sci.* **2020**.
[S3] D. Li, C. Lin, C. Batchelor-McAuley, L. Chen, R. G. Compton, *J. Electroanal. Chem.* **2018**, *826*, 117-124.
[S4] K. Aoki, K. Honda, K. Tokuda, H. Matsuda, *J. Electroanal. Chem. Interfacial Electrochem.* **1985**, *182*, 267-279.
[S5] D. R. Bates, M. Nicolet, *Publications of the Astronomical Society of the Pacific* **1950**, *62*, 106-110.
[S6] P. Vanysek, *CRC Handbook of Chemistry and Physics* **2000**, *8*.
[S7] A. J. Bard, L. R. Faulkner, J. Leddy, C. G. Zoski, *Electrochemical Methods: Fundamentals and Applications, Vol. 2*, Wiley New York, **1980**.